On the unwrapping of dispersion curves in the irreducible Brillouin zone by means of a spatial Fourier transform approach

N.B. Roozen, L. Labelle, C. Glorieux

On the unwrapping of dispersion curves in the irreducible Brillouin zone by means of a spatial Fourier transform approach.

N.B. Roozen, L. Labelle, C. Glorieux
KU Leuven, Laboratory of Acoustics, Department of Physics and Astronomy,
Celestijnenlaan 200D 3001 Leuven, Belgium.

Summary

Using Bloch-Floquet boundary conditions implies a periodicity in both the spatial and wavenumber domains, causing the numerically computed wavenumbers to be folded or aliased within the Brillouin zone. A methodology is presented to unwrap the wavenumber spectrum to extended Brillouin zones using a Fourier transform method in the spatial domain, thus providing new insights on the physical meaning and relative amplitudes of aliased wave components. In addition, a procedure is presented to identify out-of-plane (Lamb wave type) components, which are usually of interest for thin structures.

The proposed methodologies were applied to finite element based simulations of a 2D periodic reticulated structure consisting of interconnected rectangular struts with orthorombic symmetry. This reticulated structure was used as a toy model for the skeleton in porous media, focusing on the out-of-plane waves. Laser ultrasonic experiments were conducted to verify the numerical results.

Both the simulations and measurement results indicate that, in spite of bandgap features induced by the periodicity of the structure, the dispersion behavior of the out of plane Lamb wave modes in the considered type of structure is similar to the one of the Lamb waves of a homogeneous plate with thickness equal to the one of the struts, both for wavenumbers within and outside the Irreducible Brillouin Zone.

HIGHLIGHTS
- A technique is presented to unwrap dispersion curves in the irreducible Brillouin zones to the extended Brillouin zones
- A method is presented to determine the relative amplitudes of the wave components at different wavenumbers that contribute to the respective eigenmode, for any frequency of interest.
- The unwrapping method is illustrated by means of data from a numerical model, supported by experimental results.
- The dispersion relationships of Lamb wave type of modes a 2D periodic reticulated frame structure resemble quite well the ones of a homogeneous plate

KEYWORDS: periodic structures, Bloch-Floquet; spatial aliasing, Irreducible Brillouin Zone IBZ.

1 Introduction

Many studies have been dedicated to the dispersion relationships of periodic structures[1, 2, 3, 4, 5]. From an application point of view, periodic structures are quite common and therefore important, appearing in sandwich structures, porous materials, truss beams etc. Moreover, these structures exhibit interesting dispersion properties: because of the periodicity, frequency bandgaps can exist, within which wave propagation cannot occur (e.g. see [3, 5]). This phenomenon has stimulated researchers and developers to design periodic metamaterials with enhanced structural and acoustical wave insulation or absorption in a frequency range of interest, e.g. to eliminate an unwanted tonal sound component or a disturbing narrow band vibration from a spectrum.

In order to numerically analyse periodic structures, a common approach is to use a Bloch-Floquet boundary condition. This approach reduces the modeling effort and computational effort drastically, without compromising accuracy. The method exploits the periodicity of the structure in the spatial domain. As a result of the space-wavenumber duality, this implies a periodicity in the wavenumber domain as well [6].

Although this approach has been shown to be a computationally efficient way to exploit the periodicity of a structure [5, 7], application of Bloch-Floquet boundary conditions results in an ambiguity of the wavenumber, which complicates the interpretation of the computed results. As an illustration, in Kulpe et al. [8], results that are reported to be unphysical can most likely be ascribed to aliasing effects that could be overcome by a dispersion curve unwrapping approach presented further on in this paper, for the case of 2D periodic reticulated structures.

Using the proposed unwrapping procedures, a study was performed on the wave propagation in 2D periodic reticulated structures. Our incentive for this study originates in the question whether the intrinsic, microscopic elastic properties of the porous frame material can be extracted from the propagation char-

acteristics of elastic waves traveling along the foam structure. Hilyard and Cunningham [9] derived expressions that link the global static stiffness of periodic frames to the elastic modulus of the frame material, with the porosity as the key parameter of the structure. However, in many cases, the foam material exhibits relaxation behavior, and thus a frequency dependent and complex dynamic elastic modulus. Hence, a first question is whether the dynamic behavior of macroscopic vibrations and waves in a reticulated structure depends on the microscopic material modulus and porosity in the same way as it does for the static case. Alternatively, starting from a microscopic viewpoint, one can wonder to what extent the propagation of guided waves traveling along a microscopic strut in a reticulated structure is affected by the presence of interconnections with other struts. The latter question becomes particularly pertinent when the wavelength is of the order of magnitude, or longer, than the interconnection length.

In the performed study emphasis was put on out-of-plane guided wave propagation in 2D grids, which are representative e.g. for woven textile and 2D scaffolds. In literature, many papers can be found that deal with 2D spatially periodic reticulated structures, especially for in-plane vibrations (e.g. [10, 11, 12, 13, 1, 2, 4]). The results presented here, which cover Lamb wave-type out-of-plane displacements, are complementary to the ones reported in those works.

The article is organised as follows. Section 2 starts off with a brief summary of Bloch-Floquet theory. In section 2.2 a method is described how dispersion curves in the irreducible Brillouin zones can be unwrapped to extended Brillouin zones. A spatial Fourier transform is used to determine the true wavenumber, and to classify modes according to their polarization. Section 3 presents the measurement setup. Laser excitation and detection was used for the sake of efficient and flexible excitation and detection of the out-of-plane waves in a wide range of wavelengths, ranging from the strut thickness d to a multiple of the interconnection distances L_1 and L_2 [14]. The measured wave dispersion results are compared with the ones obtained by numerical simulations. Special attention is given to the particular effects of periodicity, and to the comparison of the dispersion curves of the periodic structure with the ones of an equivalent plate, made of the same material, and with the same thickness as the struts. Conclusions are drawn in Section 4.

2 Dispersion and Bloch-Floquet theory

Bloch-Floquet's theorem [15, 16] expresses that the propagation of a wave from cell to cell does not depend on the cell location within the periodic lattice. Following Hussein [17], the displacements of two adjacent Representative Elementary Volume's (REV's) of the lattice can be written as

$$\mathbf{u}\left(\mathbf{r}+\mathbf{d},\mathbf{k}\right)=\mathbf{u}\left(\mathbf{r},\mathbf{k}\right)e^{i(\mathbf{k}^T\mathbf{d})} \tag{1}$$

where $\mathbf{r}=\{x,y,z\}$ is the position vector, $\mathbf{u}=\{u_x,u_y,u_z\}$ the displacement vector, $\mathbf{d}=\{d_x,d_y,d_z\}$ the lattice vector, $\mathbf{k}=\{k_x,k_y,k_z\}$ the wave number vector, and $i=\sqrt{-1}$. The real part of the wave number vector $\mathbf{k}$ reflects the phase velocity, while the imaginary part reflects the attenuation of the wave. By virtue of Bloch-Floquet's theorem, wave propagation through the entire lattice can be described by considering a single REV only, with obvious reductions of the computational load. Assuming a lossless medium, the discretized equations of motion of the REV can be written in matrix form as

$$\left(\mathbf{K}-\omega^2\mathbf{M}\right)\mathbf{u}=\mathbf{f}_i+\mathbf{f}_e \tag{2}$$

where $\mathbf{K}$ is the dynamic stiffness matrix of the REV, $\mathbf{M}$ the mass matrix of the REV and ω the angular frequency. The right hand side of the equation represents the force vector acting on the REV. The force vector can be decomposed into an internal $\mathbf{f}_i$ and an external force vector $\mathbf{f}_e$.

Exploiting equation (1), a constraint relation can be devised that links the displacements of the edges at either side of the REV. The constraint relation is described by the lattice vector $\mathbf{d}$, and is used to reduce the number of equations of motion. It can also be shown that the application of Bloch's procedure eliminates the internal forces $\mathbf{f}_i$ [18]. The reduced equations of motion read

$$\left(\tilde{\mathbf{K}}-\omega^2\tilde{\mathbf{M}}\right)\tilde{\mathbf{u}}=\tilde{\mathbf{f}}_\mathbf{e} \tag{3}$$

where $\tilde{\mathbf{K}}$, $\tilde{\mathbf{M}}$, $\tilde{\mathbf{u}}$ and $\tilde{\mathbf{f}}_\mathbf{e}$ are the reduced stiffness and mass matrices and the reduced displacement and external force vectors, respectively. The eigenvalue problem of the lattice structure can be formulated by setting the external forces $\tilde{\mathbf{f}}_e$ to zero:

$$\left(\tilde{\mathbf{K}}-\omega^2\tilde{\mathbf{M}}\right)\tilde{\mathbf{u}}=\mathbf{0} \tag{4}$$

Solving Eq. (4) for a range of wavenumber vectors $\mathbf{k}_i$ results in sets of eigenfrequencies $f_{i,j}$ and eigenmodes, with respective phase velocities, real part, $\mathbf{c}_{i,j}=2*\pi*f_{i,j}/\operatorname{Re}\{\mathbf{k}_i\}$.

2.1 Selection of out-of-plane modes.

Although the unwrapping methodology that will be presented in Section 2.2 is applicable to any periodic structure, 2D or 3D, and any kind of mode, in this article eigenmodes of 2D structures will be considered. The set of eigenmodes is further narrowed down to eigenmodes with dominant out-of-plane motion, in view of allowing comparison with available

experimental results on 2D grids, which yielded the out-of-plane displacements only. In this section we elaborate on an approach to select out-of-plane eigenmodes from a set of eigenmodes that result from a finite element analysis.

For the sake of simplicity and straightforward validation with an analytical model, we have started off with a solid plate to illustrate the selection of out-of-plane eigenmodes (this section) and the unwrapping approach (Section 2.2).

A REV with dimensions 7.5 × 7.5 mm in a polyamide plate of $t = 1.1mm$ thickness, Young's modulus $1.8GPa$, Poisson's ratio 0.4 and density $1200kg/m^3$ was modeled by means of the FEM, applying Bloch-Floquett boundary conditions at the edges of the REV. Varying the wavenumber in one lateral direction of the REV, the eigenvalue frequencies were computed, thus obtaining the dispersion relations. The prescribed wavenumber in the x-direction was varied between $0 < k_x < \pi/d_x$ =418.9 rad m^{-1}, with $d_x = 7.5$ mm. The wave propagation is considered in one direction only, the x-direction, which reduces the Bloch-Floquett boundary conditions to $\mathbf{u}(x + d_x) = \mathbf{u}(x)$. As the plate was assumed to be lossless, only real values of the wavenumber were considered. The solutions to Eq. 4 that yielded real eigenvalues ω, for the prescribed wavenumbers k_x, are shown in Figure 1.

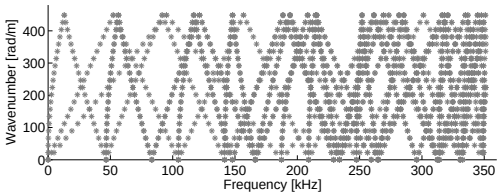

Figure 1: Numerical eigenfrequencies found for prescribed wavenumbers, for a 1.1mm thick polyamide solid plate.

For every (ω,k) solution found by the FE eigensolver, the amplitudes of the Out-Of-Plane (OOP, in the z-direction) and In-Plane (IP, in the x- or y-direction) components of the corresponding displacement field were evaluated and the ones with an OOP/IP ratio larger than 50, were retained. For the selected OOP modes, the sign of the ratio between the u_z displacements at the top and bottom surface of the plate was used to classify the modes into symmetrical (S_n) and antisymmetrical (A_n) ones, as illustrated in Figure 2.

Using this approach, the modes were sorted according to their symmetrical/antisymmetrical, and OOP/IP character, as illustrated in Figure 3. Besides the well-known symmetric (S0, red symbols) and antisymmetric (A0, blue symbols) branches of OOP Lamb modes known for a plate, other branches of OOP as well as IP modes modes are apparent (gray symbols).

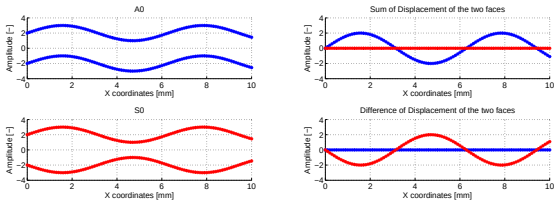

Figure 2: Schematic representation of the methodology used to distinguish A_0 and S_0 based on the (anti-) symmetry of the Out-Of-Plane displacement at the top and bottom plate interfaces.

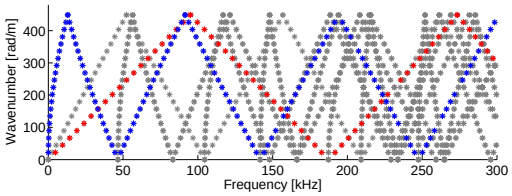

Figure 3: Eigenmode (ω,k) pairs of a 1.1mm thick polyamide solid plate found by an FE eigensolver. The OOP A_0 and S_0 mode are indicated by blue and red crosses, respectively. The IP modes are indicated by grey crosses.

2.2 Unwrapping of dispersion curves from the IBZ to extended Brillouin zones

Consider a structure that is periodic in the $x-$direction with spatial period d_x. As a result of the space-wavenumber duality, the dispersion relation of a spatially periodic mechanical system is periodic in wave number domain as well [6]. The dispersion curves are periodic in the k_x direction, with the reciprocal lattice vector

$$\mathcal{K} = 2\pi/d_x. \tag{5}$$

as period. Thus, any frequency-wavenumber pair (ω,k_x) will have a multiple of counterpart frequency-wavenumber pairs

$$(\omega, k_x + \mathcal{K}m), \tag{6}$$

where m is an arbitrary integer. The part of the wavenumber domain defined by

$$[0, \mathcal{K}/2] \tag{7}$$

completely defines the dispersion relation of a periodic structure. This part of the wavenumber domain is called the Irreducible Brillouin Zone (IBZ).

This aliasing phenomenon has the advantage that the full wave behavior of the structure is condensed in the IBZ, which is limiting the calculation effort. Using relationship 6, the dispersion curves can be replicated in the wave number domain, for all frequencies, from

the IBZ to extended Brillouin zones, by adding multiples of $\mathcal{K}$ to the wavenumbers k_x in the IBZ. However, it is a challenge to determine to what extent modes at different wavenumbers, replicated to extended Brillouin zones, contribute to eigenmodes of the frame for different frequencies.

An example of an unwrapped result for the A_0 and S_0 OOP modes in the full plate under consideration is shown in Figure 4. The values of m were chosen such that the well-known $A0$ and $S0$ dispersion curves were obtained, matching the non-aliased physical reality.

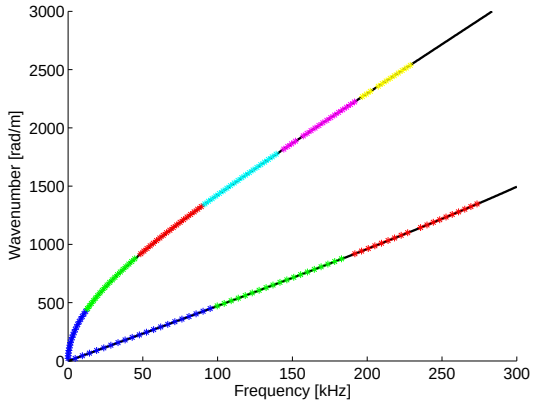

Figure 4: Unwrapping Bloch-Floquet OOP model results for a solid plate by means of a spatial Fourier transform approach.

Automated determination of m-values that correspond with a respective non-aliased physical solutions is not trivial, in particular in more complicated reticulated structures, where the physical nature of different modes is not known *a priori*. In order to address this difficulty and find appropriate m values, we have taken a step back. We considered for each wavenumber-frequency pair in the IBZ the corresponding displacement pattern in the unit cell, and periodically extended it over a large number of cells (typically about 800) in the propagation direction x, consistent with the Bloch-Floquet boundary condition, Eq. 1:

$$\mathbf{u}\left(x+nd_x\right)=\mathbf{u}_{IBZ}\left(x\right)e^{i(nk_xd_x)}, n=1...800 \quad (8)$$

Using this procedure, the respective structural mode was replicated in the spatial domain over a wide range of possible (eigenmode) wavelengths, up to the longest ones of interest. This replication process was performed for every eigenfrequency that resulted from the finite element solution that was obtained for a specific Bloch-Floquet boundary condition (i.e. for a specific prescribed wavenumber k_x). Next, we described the waveform of each structural mode as a sum of sinusoidal (Fourier) wave forms. Note that due to the 2D periodicity of the frames, with side branches repeating every distance d_x, the structural modes deviate from simple sinusoidal shapes; a multitude of Fourier components are required to describe their displacement fields. The amplitudes of these wavenumber components were determined by taking a spatial Fourier transform of the periodically extended displacement pattern. The non-aliased components of the eigenmode were then identified from the computed Fourier components.

Note that the above described procedure can be extended and applied to structures that are periodic in 2 or 3 dimensions.

To illustrate the use of a spatial Fourier transform to 'de-aliase' the computed eigenmode, we consider the 1.1 mm polyamide plate, whose dispersion behavior in the IBZ was shown in Figure 1. Eigenmodes were computed by prescribing a Bloch-Floquet wavenumber in the IBZ equal to $k_x = 230.4$ rad/m. Figure 5A shows the dispersion curves after applying Bloch's theorem to replicate the dispersion curves in the IBZ to the extended Brillouin zones by shifting the wavenumbers by $\mathcal{K}m$, for a number of m-values of interest, exploiting the periodicity in the wavenumber domain, Eq. 6. To identify which value of m constitutes the true 'non-aliased' component of the numerically computed eigenmode at a specific eigenfrequency (as obtained for a specific Bloch-Floquet boundary condition), the extended eigenmode was transformed from physical space (x) to wavenumber domain (k) by means of a spatial Fourier transform. The result of this transformation is illustrated, as an example, for an eigenfrequency of 170.4 kHz in Figure 5B. This figure clearly shows that, in this case of a simple plate, only one specific wavenumber, k_x=2041 rad m^{-1} stands out, which corresponds to a physical, 'non-aliased' mode. Note that the IBL runs up to π/d_x=418.9 rad m^{-1} ($d_x = 7.5$ mm). Thus, the true wavenumber lies in the extended Brillouin zone. All other wavenumbers (corresponding to other integer values of m) can be associated with non-physical, aliased components: Figure 5A shows that they have a negligible amplitude, more than 70 dB smaller than the physical one. As expected, the dominant k, f-pair $\omega/(2\pi)$=170.4kHz, k=2041 rad m^{-1} corresponds to the A_0 mode for an infinite plate, which is the only antisymmetric physical A0 mode possible. The negligibly small peaks in the Fourier spectrum can be considered as numerical artifacts. We have verified that the true 'non-aliased' S0-mode can be recovered in a similar manner.

In a next step, the above described procedure for "de-aliasing" wavenumbers in the IBZ, by re-assigning them to their proper extended Brillouin zone value, was also applied to a simple polyamide beam with rectangular cross section (1.1mm x 1.1mm). Fig. 6 shows that the procedure leads to the proper dispersion curves, as known from the not-periodized, analytical modeling of the infinite plate and beam.

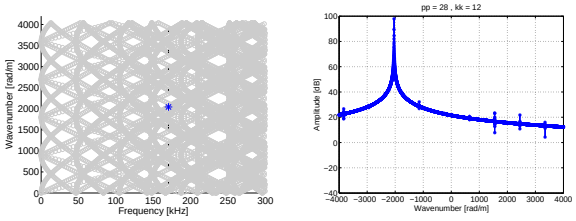

A) B)

Figure 5: Illustration of the unwrapping process using a search of a peak in a spatial Fourier transform of the displacement field of the solid plate model, for eigenmodes computed by prescribing a Bloch-Floquet wavenumber in the IBZ equal to k_x = 230.4 rad/m. A): k,f dispersion plot of all eigenmodes found, replicated using Eq. 6; B): spatial Fourier transform spectrum of an eigenmode with an eigenfrequency of 170.4 kHz, after replicating the displacement pattern to 800 REV-cells (exploiting Eq. 8), showing one dominant peak at k=2041 rad m^{-1}.

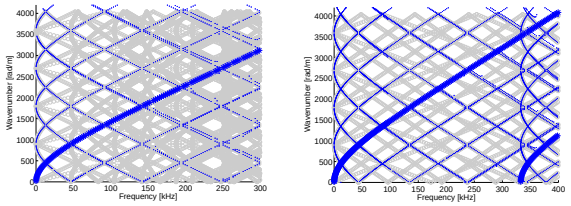

A) B)

Figure 6: A): Dispersion curve (A_0 mode) from a FEM model, including 'aliased' A_0-components, for a 1.1mm thick plate. B): Dispersion curve for a 1.1x1.1mm^2 cross section beam made of polyamide material. The true A_0-components clearly have a larger magnitude, as represented by the symbol size, than the 'aliased' A_0-components. For the beam, also the A_1 mode, including its 'aliased' components stands out, at frequencies above 325 kHz.

2.2.1 Dispersion curves of reticulated structures.

In this section, four 2D orthorombic reticulated structures, consisting of interconnected beams with square cross section, periodically arranged in a plane as shown in Figure 7, are considered. A top view of the investigated REV's, which had different values of the WH-ratio (ratio between the width and height) of the 2D, in plane cross section unit cell, are schematically represented in Figure 8. The thickness of the beams is 1.1mm.

Figure 9A shows all the modes within the IBZ, together with the replicated ones in the extended Brillouin zones (exploiting Eq. 6), for the frame structure with an width-height ratio (WH-ratio) of 1:1 (Fig. 8A, blue frame). Considering e.g. the computed eigenmode at a frequency of 159.5kHz, and a

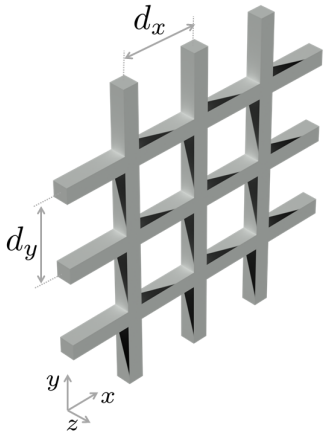

Figure 7: 3D perspective view of a grid with struts having rectangular cross section.

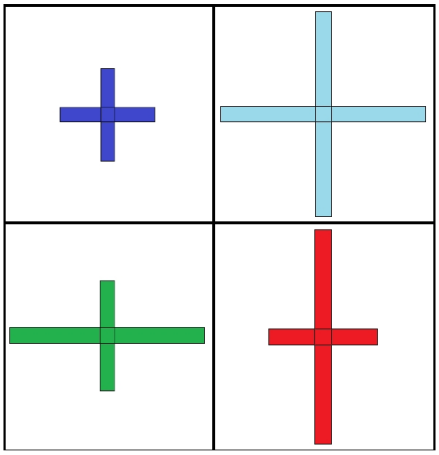

Figure 8: Top view of the Finite Element model of the investigated frame models, which differ in their value of the WH-ratio of the unit cell, i.e., the ratio between the width and height of the unit cell.

prescribed Bloch-Floquet wavenumber k_x=230.4 rad m^{-1}, the wave components of this eigenmode were extracted by means of the spatial Fourier transform approach described in the previous section. Figure 9B shows, for this eigenmode, the spectral amplitude of the Fourier components of this mode, which spectrum has a rather limited spectral resolution. Figure 9C shows the wavenumber spectrum, as obtained from a spatial Fourier transform of the replicated displacement field over 800 unit cells, exploiting Eq. 8. Note that the larger the number of unit cells considered, the better is the wavenumber resolution. Fig. 9D shows the computed structural eigenmode. In order to get an idea on the relative magnitudes of the different wavenumber contributions, the contribution of the most dominant wavenumber, k_x=1905m$^-$1 (which equals the IBZ wavenumber k_x=230rad/m plus two times the reciprocal lattice spacing $\mathcal{K} = 2\pi/d$=839 rad/m), shown separately (blue asterisks). Interest-

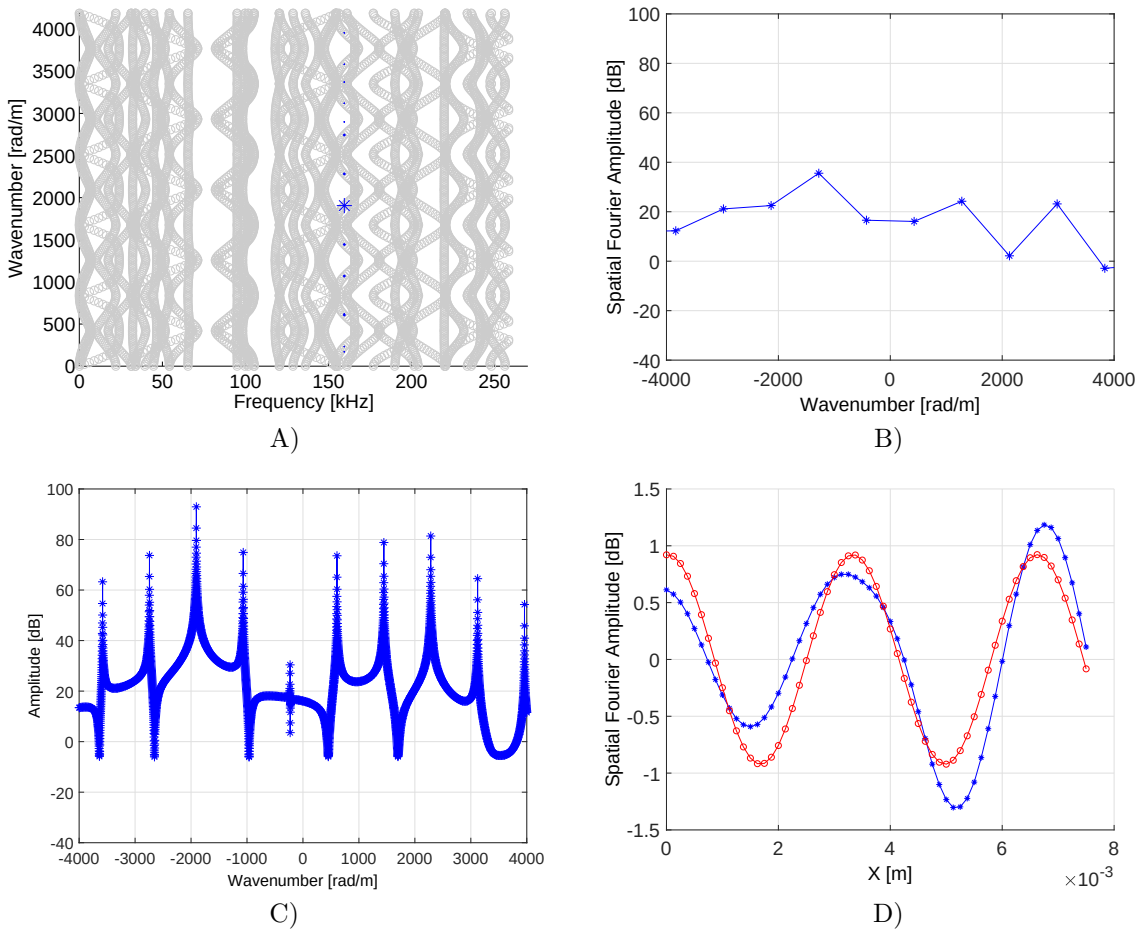

Figure 9: Illustration of the unwrapping process using a search of a peak in the spatial Fourier transform of the displacement field of the numerical 'WH-ratio 1:1' frame model, for a frequency of 159.5 kHz and a prescribed Bloch-Floquet wavenumber k_x=230.4 rad/m. A): The full IBZ and extended IBZ dispersion plot. The size of the blue marker indicates the amplitude of the spatial Fourier component at a frequency of 159.5 kHz B): Spatial Fourier transform spectrum using the displacement pattern of the REV cell (i.e. **one** unit cell only). C): Spatial Fourier transform spectrum, after replicating the displacement pattern to 800 REV-cells (exploiting Eq. 8). D): Out of plane displacement pattern within a REV, including only the most dominant wave component of Fig. 9C (red circles), and including all wave components of Fig. 9C (blue asterisks)

ingly, in this case, this contribution, as well the other largest contributing wavenumbers, are all lying out of the IBZ, in the extended Brillouin zones. Note that due to the different absolute values of the negative and positive wavenumbers, the amplitude spectrum is not symmetric around k_x=0.

Figure 10 shows an overview of the k,ω magnitude plots obtained for the replicated displacement patterns of OOP antisymmetric modes, for the 3 geometries of Fig. 8, with WH-ratio values 1/1, 2/2, 1/0.5, 0.5/1. In general it is observed that an eigenmode as computed from a model of a repetitive frame structure is constituted of a plentitude of Fourier wave components of which a small number are dominant. For the grids considered in this study, the dominant Fourier wave components typically have wavenumbers that are close to the wavenumbers of a homogeneous plate with the same material properties and the same thickness.

In all cases shown in Fig. 10, the magnitudes of the Fourier components are strongest near the A_0 branch of the simple infinite plate with thickness equal to the thickness of the rectangular beams of which the frames are composed. This implies that, similarly to the case of the simple plate, also in a 2D frame geometry, the bending stiffness of the individual polyamide beams in the frame can be approximated by fitting the dominant modes to a simple plate model. In other words, the trend line through the dominant (k,ω) pairs existing in the frame dispersion plot is a good approximation for the dispersion of the main flexural mode of a 2D reticulated structure is a good approximation for the A_0 mode of a homogeneous plate with the same material properties and the same thickness. Interestingly, the correspondence is also valid for very small wavenumbers, for which the wavelength is much

longer than the REV size. Contrary to the considered case of out-of-plane displacements, in this limit, and in the very limit of zero wavenumber corresponding to the case of static deformations, it has been shown that the in-plane elastic behavior of the frame strongly depends on the structural porosity (i.e. the filling fraction) [9, 1, 2].

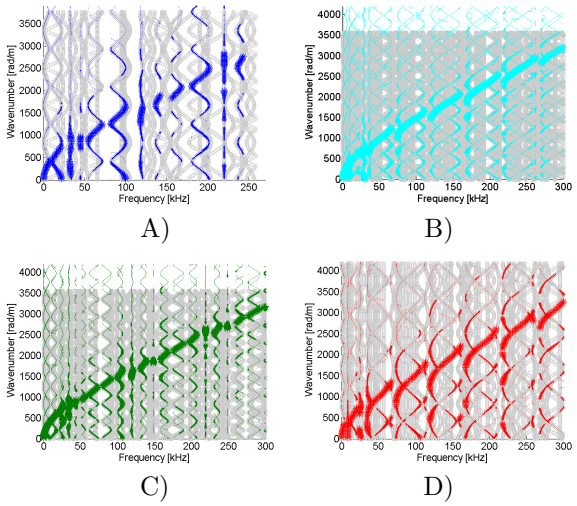

Figure 10: Dispersion curves of the A_0 mode. A) WH-ratio 1:1, 7.5mm strut length; B) WH-ratio 2:2, 15mm strut length; C) WH-ratio 2:1, 15mm strut length; D) WH-ratio 1:2, model 7.5mm strut length. The colors in this figure corresponds to the color coding in Fig. 8.

Fig. 10 shows that when the struts are long with respect to the strut thickness, the bandgaps are narrower (compare e.g. 10C with 10A) and the dispersion curve deviations (with respect to the classical dispersion curves of a simple plate) in their vicinity are less pronounced. This is consistent with the maximum wavenumber value for the Brillouin zone being inversely proportional with the size of the unit cell, i.e. the strut length ($\mathcal{K} = 2\pi/d_x$). In the limit of infinite strut length, a simple beam structure would be obtained, while the bandgap features would disappear.

Looking at the opposite case of a short strut length (Fig. 10A and Fig. 10D), the dispersion curve deformations are roughly twice as large and the bandgaps are wider. Note also that the WH-ratio 1:1 (blue) points that are not corresponding with the A0 mode belong to a torsional vibration mode of the strut (leading to an out-of-plane displacement component). Such torsional modes are visible in the following frequency ranges: 30 kHz - 50 kHz; 110 kHz - 130 kHz; 210 kHz - 250 kHz.

3 Experimental analysis

Dispersion measurements were performed on a 3D printed polyamide frame consisting of rectangular beams with a cross section of 1.1mm x 1.1 mm and equal unit cell length and width of 7.5mm (WH-ratio 1), as shown in Fig. 11. The nominal material properties of the polyamide material were estimated as: Young's modulus = between 1 and 2 GPa, density = 1200 kg/m3, Poisson's ratio = 0.4.

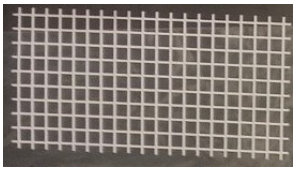

Figure 11: 3D printed polyamide grid sample, with square cross section struts, 1.1 mm × 1.1 mm, a unit cell WH-ratio of 1/1, and a periodic length scale d_x of 7.5 mm.

We have made use of photoacoustic excitation (see Fig. 12) of guided elastic waves by illuminating a spot on the sample with light pulses from a 10 ns Spectra Physics Quantaray Nd:YAG laser with a 10 Hz repetition rate. In this approach, illumination of the material with laser pulses results in partial optical absorption of the light energy, heating and thermal expansion. Due to the impulsive character of the induced stress, this results in elastic waves to be launched along the struts, in this specific case every 0.1 second. Although the generation bandwidth of 10 ns pulses is of the order of 100MHz, due to material damping, dynamic range limitations of the Polytec Laser Doppler Vibrometer (sensor head OFV-353 with controller in displacement mode, with a sensitivity of 50nm/V), and a finite laser spot size, the spectrum of the detected signal was limited to the 50 kHz-500 kHz range.

The phase velocity of the generated waves was determined from their spatiotemporal behavior. A scanning stage from APT Thorlabs was used to scan the exciting Nd:YAG laser beam along the sample, thus systematically varying the distance x between the excitation and detection position. Signals were recorded on an oscilloscope (Lecroy LC564A) and acquired by a Labview program for every position of the scan, resulting in a signal matrix S(x,t). A 2D Fourier transform of this matrix was taken, resulting in an amplitude map —S(k,f)—, from which k,f-pairs satisfying the dispersion relations were extracted.

Figure 13A depicts the spatiotemporal behavior of photoacoustically excited waves along the grid. Two right-running (arrival time increasing with pump-probe distance x) with different velocity (slope $\Delta x/\Delta t$), and, from x=120 mm onwards, their reflections can be distinguished. The fastest wave

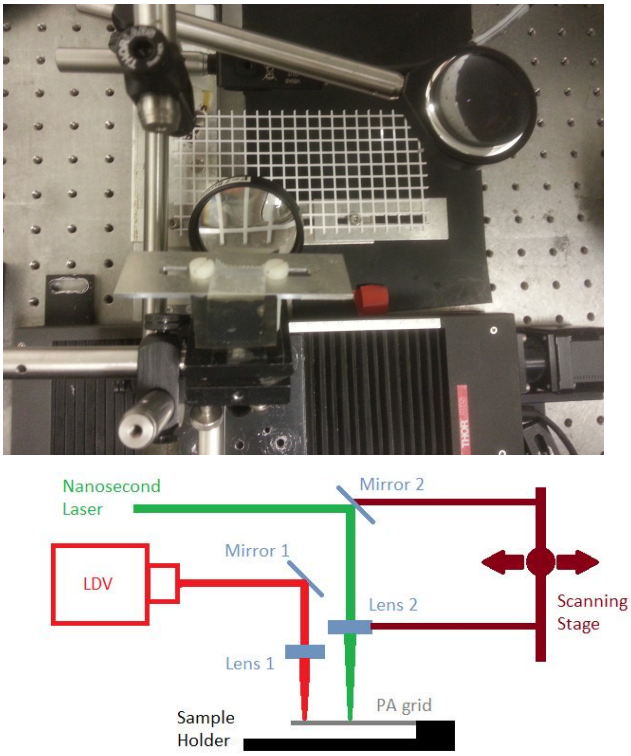

Figure 12: Experimental test setup.

packet, reaching the end position ($x = 120$mm) in about 100ms, keeps its width, implies that this is the S0-wave, with limited dispersion. The slower wave spreads out more in time with increasing detection distance, indicating A0-character.

Figure 13B shows the result of a 2D FFT, giving a color map of the amplitude spectrum versus wavenumber and frequency, (k, ω). The A0 and S0 modes of wave propagation are clearly visible, till about 350 kHz and 400kHz respectively.

A peak search along the k-axis for each frequency was performed to extract the dispersion curves k(f), shown in Figure 13C for the A0 and S0 mode. As a reference, also the analytically calculated dispersion curves of the A0 and S0 modes of an infinite polyamide plate of 1.1mm thickness are indicated by black and gray lines, respectively. Like the numerical simulations, the experimentally obtained dispersion curves for reticulated structures match the dispersion curve of the plate reasonably well. The dispersion curve of the plate, in turn, is known to be very similar to the one of the individual beams. This allows the material properties of the 2D periodic frame type of structure considered in this study, can be fitted (in approximation) from measurement data, using a homogeneous plate of the same thickness. It should be noted, however, that the 2D periodicity of the frames also causes a repetitive deviation from the ideal homogeneous plate dispersion curves, as becomes evident from Fig. 13C,D.

In Fig. 13D the experimental results of Fig. 13C, here in magenta circle marker, are compared with numerical simulation results using a FE-model of the frame structure, selecting out-of-plane modes and extending beyond the IBZ as explained in Section 2. The black dashed lines indicate the Brillouin zones.

4 Conclusions

Bloch-Floquet's theorem permits the dispersion relations of periodical reticulated structures to be computed with low computational effort, by exploiting the accompanying periodicity in wavenumber domain. The application of the theorem, which allows to restrict the search of eigenmodes to the Irreducible Brillouin Zone (IBZ), can be considered as a beneficial exploitation of spatial aliasing.

In this work, we have shown that by taking a spatial Fourier transform of the Bloch-expanded displacement field, the true, non-aliased Fourier components of the constituting wave components can be determined. In addition, the relative amplitude of these components to the displacement field of the mode under consideration can be determined. Unwrapping the aliased components to extended Brillouin zones is useful to correctly classify and interpret the physical meaning of the numerical eigenmodes that result from the Bloch-Floquet model. The unwrapping methodology is applicable to any structure, 2D or 3D, and to any kind of mode.

Although wave propagation along rectangular struts in a 2D spatially periodic reticulated structure is affected by strut interconnections, the wavenumbers that have the highest amplitudes in the Fourier decomposition of the eigenmodes of the frame at different frequencies, are close the wavenumbers of waves propagating in infinite struts, and in an infinite, monolithic, "equivalent" plate that has the same thickness as the struts.

Laser ultrasonic experiments were performed on a 3D printed polyamide planar frame with grid size of 7.5 mm, and a strut thickness of 1.1 mm. Photoacoustically excited guided waves were measured by performing pump-probe distance scans. The strengths of the experimentally assessed out-of-plane wavenumber-frequency pairs, obtained by 2D Fourier transforming the spatiotemporal dependence of the experimental signals, were found to be consistent with the numerically predicted ones.

On the basis of both numerical simulations and experimental results, it can be concluded that, in spite of deviations due to the periodic structure, the dispersion curves of the out of plane modes are still very similar to the out-of-plane Lamb waves of a plate that is "equivalent " with the rectangular beam structure. As a consequence, the microscopic bending stiffness of a reticular frame can be approximated by fitting the measured dispersion curves of out-of-plane modes

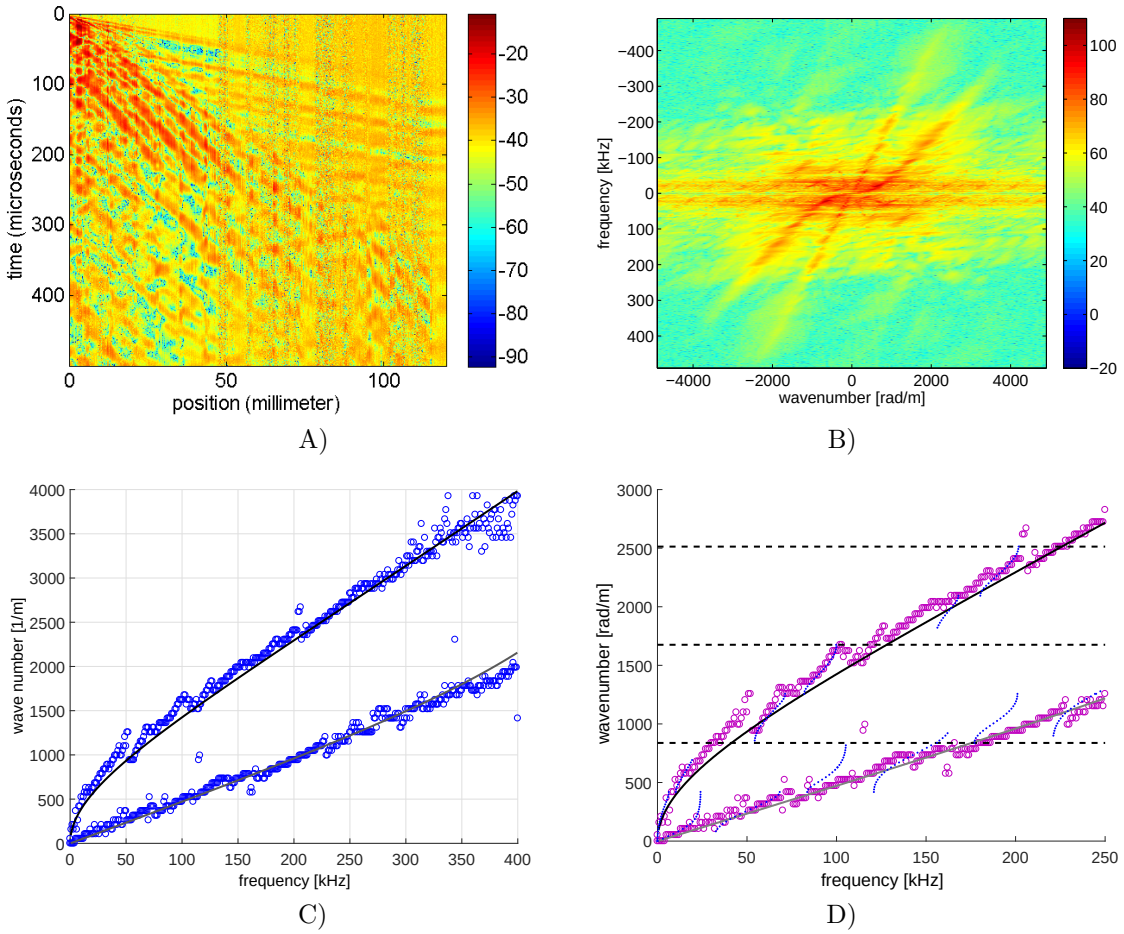

Figure 13: Regular frame structure WH-ratio 1:1, strut length 7.5mm. A) Measured spatiotemporal map of the photoacoustically generated waves. B) Measured amplitude map in wavenumber-frequency domain. C) Extracted frequency-wavenumber pairs from the measurement data with significant amplitude (blue circles) and numerically predicted dispersion relationship for an equivalent plate, revealing the presence of both A0 and S0 modes. D) Comparison between experimentally obtained dispersion curves (magenta circles) with numerically computed ones for an equivalent plate (black and gray solid curves) and for the Bloch-Floquet model of the periodic reticulated structure showing the unwrapped results (dotted blue curves), for both A0 and S0 modes.

on the numerically obtained dispersion curves of a homogeneous, equivalent plate. This adequate simplification is very promising for porous material analysis. In common porous materials (arranged in a 2D grid), the struts are not arranged in a periodical frame, so that there is no reason for the existence of bandgaps in the dispersion plots. This suggests that in such a disordered reticulated structure, compared to the investigated periodical grids, the dispersion curves can be expected to be even more similar to the ones of the infinitely extrapolated individual struts. The elastic properties of the microscopic strut material can thus be inferred from the dispersion behavior of out-of-plane polarized waves propagating along the macroscopic frame.

5 Acknowledgement

This project has received funding from the European Union's Horizon 2020 research and innovation programme under the Marie Sklodowska-Curie RISE project PAPABUILD, grant agreement No 690970, and from Marie Sklodowska-Curie COST Action DENORMS, grant agreement No CA15125. The authors are grateful to the R&D team at Huntsman, Sterrebeek for fruitful discussions.

References

[1] C. Chesnais, C. Boutin, S. Hans, Effects of the local resonance on the wave propagation in periodic frame structures: Generalized Newtonian mechanics, The Journal of the Acoustical Society of America 132 (2012) 2873.

[2] C. Boutin, A. Rallu, S. Hans, Large scale modulation of high frequency acoustic waves in periodic porous media, The Journal of the Acoustical Society of America 132 (2012) 3622.

[3] E. Baravelli, M. Ruzzene, Internally resonating lattices for bandgap generation and low-frequency vibration control, Journal of Sound and Vibration 332 (2013) 6562–6579.

[4] C. Boutin, L. Schwan, S. Dietz, Elastodynamic metasurface: Depolarization of mechanical waves and time effects, J. Appl. Phys. 117 (2015) 064902.

[5] S. Sorokin, O. Ershova, Plane wave propagation and frequency band gaps in periodic plates and cylindrical shells with and without heavy fluid loading, Journal of Sound and Vibration 278 (2004) 501–526.

[6] M. I. Hussein, M. J. Leamy, M. Ruzzene, Dynamics of Phononic Materials and Structures: Historical Origins, Recent Progress, and Future Outlook, Applied Mechanics Reviews 66 (4).

[7] A. Palermo, A. Marzani, Extended bloch mode synthesis: Ultrafast method for the computation of complex band structures in phononic media, International Journal of Solids and Structures 100-101 (2016) 29–40.

[8] J. A. Kulpe, K. G. Sabra, M. J. Leamy, Bloch-wave expansion technique for predicting wave reflection and transmission in two-dimensional phononic crystals, The Journal of the Acoustical Society of America 135 (4) (2014) 1808–1819.

[9] N. Hilyard, A. Cunningham, Low density cellular plastics: Physical basis of behaviour, Springer, 1994.

[10] S. Gonella, M. Ruzzene, Analysis of in-plane wave propagation in hexagonal and re-entrant lattices, Journal of Sound and Vibration 312 (1-2) (2008) 125–139.

[11] A. S. Phani, J. Woodhouse, N. A. Fleck, Wave propagation in two-dimensional periodic lattices, The Journal of the Acoustical Society of America 119 (4) (2006) 1995–2005.

[12] M. J. Leamy, Exact wave-based Bloch analysis procedure for investigating wave propagation in two-dimensional periodic lattices, Journal of Sound and Vibration 331 (7) (2012) 1580–1596.

[13] L. Junyi, V. Ruffini, D. Balint, Measuring the band structures of periodic beams using the wave superposition method, Journal of Sound and Vibration 382 (2016) 158–178.

[14] L. Labelle, N. Roozen, J. Vandenbroeck, S. Akasaka, C. Glorieux, Elastic characterization of polymer fibers by laser Doppler vibrometry, Optics and Lasers in Engineering 99 (2017) 88–97.

[15] F. Bloch, Über die Quantenmechanik der Elektronen in Kristallgittern, Z. Phys. A, Hadrons Nucl. 52 (1929) 555–600.

[16] L. Brillouin, Wave Propagation in Periodic Structures, McGraw-Hill Book Company, 1946.

[17] M. I. Hussein, Reduced Bloch mode expansion for periodic media band structure calculations, Proceedings of the Royal Society A - Mathematical Physical and Engineering Sciences 465 (2109) (2009) 2825–2848.

[18] F. Farzbod, M. J. Leamy, The treatment of forces in Bloch analysis, Journal of Sound and Vibration 325 (3) (2009) 545–551.